BIOPHYSICS AND BASIC BIOMEDICAL RESEARCH – Note

Magnetic Resonance in Medicine 66:264–269 (2011)

Quantitative Magnetization Transfer Studies of Apoptotic Cell Death

Colleen Bailey,[1,2]* Kimberly L. Desmond,[1,2] Gregory J. Czarnota,[1–3] and Greg J. Stanisz[1,2]

Magnetization transfer measurements were performed on samples of acute myeloid leukemia cells at early (36 h post-cisplatin treatment) and late (48 h posttreatment) stages of apoptosis. Magnetization transfer ratio was calculated and a two-pool model was fitted to data at two powers and 16 offset frequencies of saturation pulse. No parameters changed significantly at early stages of apoptosis. At late stages, changes in magnetization transfer ratio were not significant, but quantitative model parameters showed a decrease in macromolecular proton fraction, M_{0B}, and an increase in the T_2 relaxation time of free water. Analysis also indicated an increase in the ratio $R \times M_{0B}/R_{1A}$, where R is the exchange rate between free water and macromolecular protons and R_{1A} is the T_1 relaxation rate of free water. Changes in the magnetization transfer spectrum were largely attributable to differences in the free water pool and did not occur any earlier than changes in the average T_1 relaxation time, T_{1obs}. Magn Reson Med 66:264–269, 2011. © 2011 Wiley-Liss, Inc.

Key words: magnetization transfer; apoptosis; tumour response; quantitative MRI

Apoptotic cell death is an important indicator of the efficacy of cancer therapy (1,2) and imaging markers of apoptosis have the potential to monitor patient response throughout treatment. Apoptotic cell death produces changes at the molecular and cellular levels. These include breakdown of proteins and changes in synthesis levels, which can be observed by ^{13}C spectroscopy (3), changes in the size of the intracellular and extracellular free water pools as observed with MR contrast agents (4) and diffusion measurements (5,6), changes in pH (7), and changes in lipids detected by molecular imaging (8–10) and NMR spectroscopy. In particular, spectroscopy studies have attributed an increase in the CH_2/CH_3 signal intensity ratio to an increase in mobile lipids (11–13).

Magnetization transfer (MT) is an MRI technique for indirect detection of macromolecular protons. Protons processing at a frequency that is offset from the water proton resonance are saturated by a radiofrequency (RF) pulse and signal from free water protons is reduced through exchange between the two proton pools (macromolecular and free water). The fraction of free water signal lost following a saturation pulse at a single offset frequency gives the MT ratio (MTR).

Because exchange can occur multiple times during RF saturation, MT can produce much larger effects than direct measurements by spectroscopy, although MTR at a single offset frequency is less specific. Specificity can be improved by quantitative MT, which models the changes produced by saturation of the water pool across a range of offset frequencies.

Previously MT has shown sensitivity to cellular-level changes including myelin content (14), ischemia (15), and development of tumors, necrosis, and hemorrhage (16). The biochemical and morphological changes of apoptosis may, in theory, alter the MT spectrum because of changes in the number of exchangeable macromolecular protons and size of the free water pool, the dynamics of the macromolecular pool, and the exchange rate (which is affected by multiple factors including accessibility of the exchange site and, for small molecules where chemical exchange is a significant contributor to the MT effect, the pH (17)). This study examines the MT effect in an in vitro model of apoptotic cell death by both MTR and quantitative MT modeling.

MATERIALS AND METHODS

Cell Culture and Sample Preparation

Flasks of acute myeloid leukemia cells (AML-5) were grown in suspension, each with 150 mL α minimal media (Invitrogen Canada Inc., Burlington, Canada), 25 mL fetal bovine serum (Fisher Scientific, Ottawa, Canada), and 5 mL penicillin and streptomycin (Invitrogen Canada Inc.). Flasks were kept at 37°C and 5% CO_2 until they reached confluence ($\sim 10^6$ cells). Cells have a doubling time of ~1.3 days.

Four flasks were treated with 10 μg mL^{-1} cisplatin 36 h before imaging. Cisplatin is a chemotherapy drug that impairs DNA replication and repair, producing apoptotic changes observable by both light and phase microscopy. Four flasks were treated with cisplatin 48 h before imaging. Four flasks were left untreated as controls.

Just before imaging, samples were prepared by combining the volumes of the four flasks in a treatment group and centrifuged at 988*g* using a fixed angle centrifuge (Beckman Coulter, Brea, CA). Excess medium was removed and cells were resuspended in a small volume (~1 mL) of phosphate-buffered saline (Invitrogen Canada

[1]Department of Medical Biophysics, Faculty of Medicine, University of Toronto, Toronto, Ontario, Canada.

[2]Imaging Research, Sunnybrook Health Sciences Centre, Toronto, Ontario, Canada.

[3]Department of Radiation Oncology, Faculty of Medicine, University of Toronto and Sunnybrook Health Sciences Centre, Toronto, Ontario, Canada.

Grant sponsors: National Cancer Institute of Canada, Canadian Institutes of Health Research, Terry Fox Programme, National Sciences and Engineering Research Council

*Correspondence to: Colleen Bailey, B.Sc., Sunnybrook Health Sciences Centre, 2075 Bayview Ave., S-Wing, 6th floor, Rm S612, Toronto, Ontario, Canada M4N 3M5. E-mail: colleen.bailey@sri.utoronto.ca

Received 15 October 2010; revised 30 November 2010; accepted 20 December 2010.

DOI 10.1002/mrm.22820

Published online 17 February 2011 in Wiley Online Library (wileyonlinelibrary.com).

Inc.). This volume was transferred to a 4-mL flat-bottomed centrifuge tube (Sarstedt, Nümbrecht, Germany) for quantitative MT experiments. Tubes were centrifuged for 2 min at 2000*g* and 6 min at 2900*g* using a swinging bucket centrifuge (Thermo Electron Corp., Asheville, NC) to produce a sample for imaging with similar cell density to a tissue environment (~70% by volume). The experiment was carried out four times ($n = 4$) to determine reproducibility.

MR Data Acquisition

MR data were acquired at 1.5 T (GE Signa, Milwaukee, WI) using a quadrature head coil. Axial slices were centered lengthwise through the tubes.

T_1 relaxation data were acquired using a two-dimensional inversion recovery sequence (18) with 128^2 acquisition matrix, pulse repetition time = 2500 ms, and echo time = 11 ms. Nine separate inversion times were used: 50, 100, 200, 300, 500, 700, 900, 1200, and 1500 ms.

A three-dimensional spoiled gradient echo sequence (pulse repetition time = 200 ms, echo time = 4 ms) preceded by an off-resonance Hanning-windowed Gaussian saturation pulse (19) (pulse width = 82 ms) was used to acquire the MT spectrum. Data were acquired for two peak powers ($\omega_1/2\pi = 427$ or 243 Hz) at 16 offset frequencies spaced logarithmically from 0.12 to 200 kHz. A 15° on-resonance excitation pulse was used to read out the signal. For all offset frequencies, this acquisition scheme achieves steady-state (defined as <0.1% change between pulse repetitions) within 20 repetitions, toward the outer edges of *k*-space.

MT images were acquired in a 64^2 matrix with a field of view 8–12 × 8–12 cm^2 (resulting in in-plane resolution 1.25–1.88 × 1.25–1.88 mm^2) and 4.5 mm slice thickness.

Data Analysis

Regions of interest were automatically selected from pixels at the bottom 10 mm of the sample tube and in the 8 mm centered horizontally in the tube to avoid partial volume effects. The signal-to-noise ratio was calculated by dividing the mean signal in the 200 kHz offset, 427 Hz peak power image by the mean signal in an empty region of interest outside the samples.

The signal in the region of interest for the nine inversion recovery images was fitted to

$$S = S_0\left[1 - (1 + a)e^{T1/T1_{obs}} + ae^{-TR/T1_{obs}}\right], \qquad [1]$$

where S_0 is the equilibrium signal that would be measured if all magnetization were transferred into the transverse plane, T_{1obs} is the average, observed T_1 relaxation time in the voxel, and a accounts for imperfections in the 180° pulse.

Quantitative MT data were fit to a two-pool model of MT (20). Macromolecular protons (pool B) are saturated with RF irradiation. Magnetization from the free water pool (pool A) and the macromolecular pool exchanges with a rate R. Each pool has a different proton fraction (M_{0A} and M_{0B}), T_1 relaxation rate (R_{1A} and R_{1B}), and T_2 relaxation time (T_{2A} and T_{2B}).

The time constant T_{2B} characterizes the width of the macromolecular line shape, which was assumed to be super-Lorentzian for these experiments, as specified for tissues (21). The fraction of free water protons, M_{0A}, was normalized to 1 by convention and the macromolecular longitudinal relaxation rate, R_{1B}, was fixed to 1 s^{-1} as an approximation because the fit is insensitive to it (22). According to Henkelman et al. (22), the longitudinal relaxation rate of the liquid pool, R_{1A}, can be calculated from the independently measured, longitudinal relaxation time, T_{1obs}.

The change in the magnetization is then described by a series of differential equations given by Sled and Pike (20, see their Eqs. 1–4). Apart from the precalculated R_{1A} value and the fixed values $M_{0A} = 1$ and $R_{1B} = 1$ s^{-1}, there remain four free model parameters to fit: R, M_{0B}, T_{2A}, and T_{2B}. In addition, the ratio of parameters characterizing free water magnetization lost through exchange to those describing the recovery by T_1 relaxation, $R \times M_{0B}/R_{1A}$, was calculated as a measure of overall MT.

MTR was calculated for the 427 Hz peak power and 2.32 kHz offset frequency:

$$\mathrm{MTR} = \frac{S_{200} - S_{2.32}}{S_{200}}, \qquad [2]$$

where S_{200} and $S_{2.32}$ are signals from the MT sequence at offset frequencies $\Delta = 200$ kHz and $\Delta = 2.32$ kHz, respectively.

Fitting errors in each of the four independent model parameters were determined by adjusting the parameter of interest and allowing the remaining parameters to vary until

$$\chi^2 \geq \chi_0^2\left[1 + \frac{n_p}{N - n_p}F(n_p, N - n_p, 0.68)\right], \qquad [3]$$

where χ^2 is the reduced χ^2 value from the fit with one fixed parameter, χ_0^2 is the reduced χ^2 value with all parameters optimized, n_p is the number of parameters in the fit ($n_p = 4$), N is the number of data points ($N = 32$), and F is the F distribution function, calculated here for a 68% confidence interval (23).

Histology

Following MR data collection, the tubes containing the cell samples were placed in 10% formalin for at least 1 week. Samples were then pushed intact out of the tubes and embedded in 3% agarose. Following paraffin embedding, 5 μm-thick longitudinal slices were cut and stained with hematoxylin and eosin (H&E). The number of apoptotic cells as a fraction of the total number of cells in the microscope field of view was determined for three fields near the center of the slice (559–859 cells counted for each sample). Apoptotic cells in stained slides were determined as those where nuclear condensation and fragmentation were visible and confirmed using TUNEL staining.

RESULTS

The average signal-to-noise ratio of the 200 kHz MT images was 108 ± 1 for data sets with 12 × 12 cm^2 field

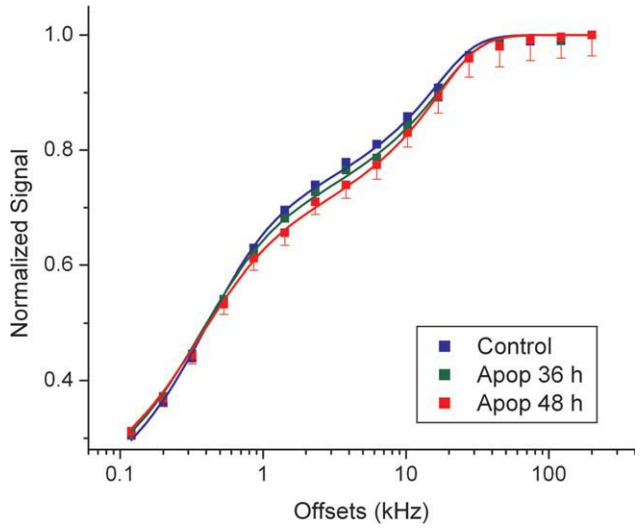

FIG. 1. MT curves for cell samples with no treatment (control), 36, and 48 h after treatment with cisplatin for $\omega_1/2\pi = 427$ Hz peak power. Lines represent fits to the data. The standard deviation of the signal across the selected region of interest is demonstrated by the error bars on the 48 h treatment points. Errors for control and 36 h time points were similar.

of view and 48.5 ± 0.2 for 8 × 8 cm^2 field of view. The MT data from a sample experiment are shown in Fig. 1. The solid lines are the fits to the data. There was excellent agreement between the fitted model and experimental data.

The average fit parameters across experiments and observed longitudinal relaxation time, T_{1obs}, are shown in Fig. 2. A two-tailed unpaired *t*-test indicated that differences between apoptotic and normal control samples become significant ($P < 0.05$) for three quantitative MR parameters—observed longitudinal relaxation time, T_{1obs}, macromolecular proton fraction, M_{0B}, and transverse relaxation time of the free water pool, T_{2A}—at 48 h after cisplatin treatment. Although some trends, such as a decrease in M_{0B} and an increase in T_{2A}, were evident in the earlier data 36 h after cisplatin treatment, the biological variation between the experiments leads to larger standard deviations such that the averages are not significantly different from control samples.

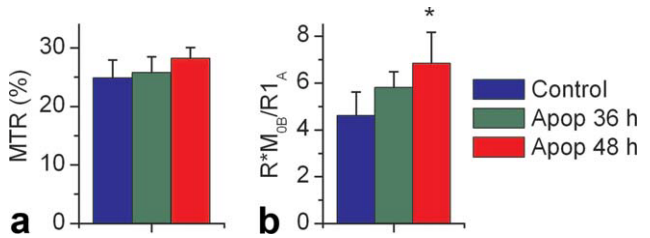

FIG. 3. Average parameters quantifying the MT effect. **a:** The average MTR at 2.32 kHz offset frequency for $\omega_1/2\pi = 427$ Hz peak power as calculated from Eq. 2. **b:** The ratio of $R \times M_{0B}$, an approximation of magnetization lost due to exchange with saturated protons, to R_{1A}, the recovery rate of magnetization due to T_1 relaxation. Error bars represent standard deviations across the four experiments and * indicates $P < 0.05$.

The average fit errors (the limits of the parameters to keep the fit within the 68% confidence interval, as given by Eq. 3) were of the same order or smaller than the standard deviations across the four experiments for the macromolecular proton fraction, M_{0B}, and the transverse relaxation time of free water, T_{2A}. For the MT exchange rate, R, and the macromolecular relaxation time, T_{2B}, fit errors were larger than the standard deviation. For R and T_{2A}, the upper limit of the fit error was larger than the lower limit. Errors were symmetric for the other two parameters.

The MTR is shown in Fig. 3. An increase in the average MTR is evident but not statistically significant. In the MT literature, the ratio $R \times M_{0B}/R_{1A}$ is often used as a fitted parameter. This ratio follows the same trend as the maximum MT effect (21) and indicated an increase that was statistically significant at 48 h and approached significance ($P = 0.09$) at 36 h.

Figure 4a–c presents a sample set of H&E stained slides for each experimental time point. A summary of the counts across all experiments is presented in Fig. 4d. Control cell samples demonstrated an apoptotic fraction of 0.03 ± 0.01 when compared with 0.35 ± 0.24 for cells 36 h after cisplatin treatment and 0.68 ± 0.14 for cells 48 h after treatment, based on counts from H&E staining. TUNEL staining showed an apoptotic fraction of 0.02 ± 0.01 for control cells, 0.23 ± 0.20 for apoptotic cells at 36 h and 0.33 ± 0.10 for apoptotic cells at 48 h.

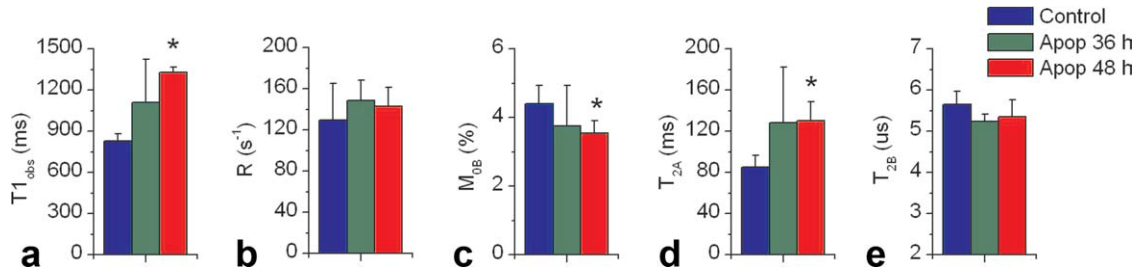

FIG. 2. Average fit parameters. **a:** Monoexponential fit to the inversion recovery data for T_{1obs} using Eq. 1. The average fit parameters for the fit to the two-pool model of MT from (20): (**b**) exchange rate R, (**c**) macromolecular proton fraction M_{0B}, (**d**) T_2 relaxation time of free water T_{2A}, and (**e**) T_2 relaxation time of the macromolecular pool assuming a super-Lorentzian line shape T_{2B}. Error bars represent standard deviations across the four experiments and * indicates $P < 0.05$.

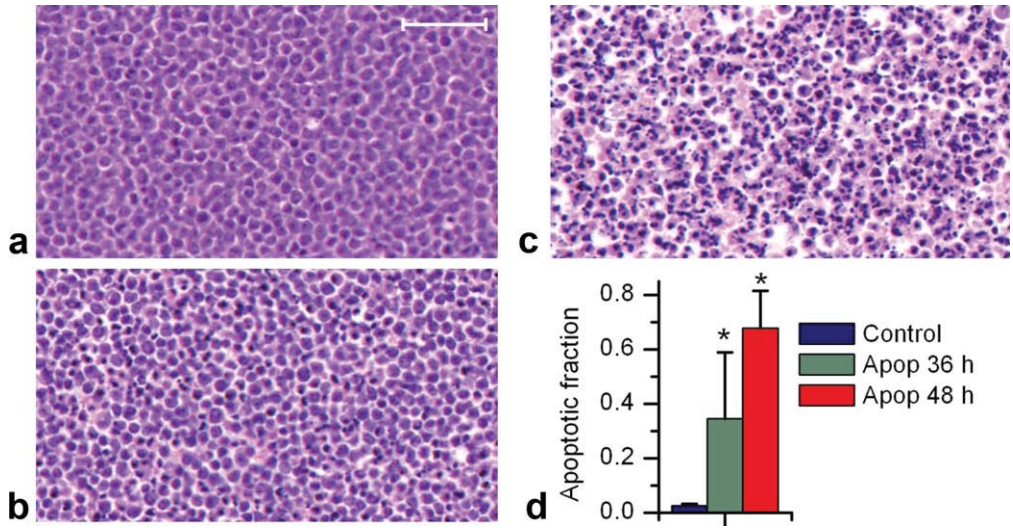

FIG. 4. Representative images of H&E-stained slides for (**a**) control cell samples, as well as (**b**) those 36 h postcisplatin treatment and (**c**) 48 h postcisplatin treatment. (**d**) The average apoptotic fraction across all experiments, as determined from counts of those cells showing condensed nuclei following H&E staining as a fraction of the total number of cells. The scale bar represents 50 μm.

DISCUSSION

We are not aware of other published studies using MT specifically to examine apoptosis. However, similar rotating frame relaxation studies that applied spin-locking RF pulses before signal readout showed prolonged $T_{1\rho}$ following treatment to induce apoptosis (24–27), which is consistent with an increased MT effect.

The fit error is of the same order or smaller than the standard deviation for the macromolecular proton fraction, M_{0B}, and the transverse relaxation time of free water, T_{2A}, indicates that these parameters can be fitted reliably. The large fit error in the MT exchange rate R has been previously observed (28), but the difficulty in fitting the macromolecular transverse relaxation time, T_{2B}, is unusual. The instability in the fit may be preventing changes in R and T_{2B} during apoptosis from being observed.

As demonstrated by the relative sizes of the error bars in Fig. 2, the standard deviations across experiments tended to be largest for the 36 h treatment time point. This is because of variation in the level of apoptotic response related to the inherent biological instability of this cell line. The apoptotic fraction 36 h after cisplatin treatment ranged from 15 to 80% across the four samples, which is reflected in the error bars on the 36 h time point in Fig. 4d. This suggests that the cellular-level changes affecting the MT signal occur near this time point, producing larger error bars as the time course of apoptosis shifts slightly with later passages of the cells being used.

As shown in Fig. 2, the longitudinal relaxation time, T_{1obs}, the MT macromolecular fraction, M_{0B}, and the transverse relaxation time of the free water pool, T_{2A}, were significantly different between the acute myeloid leukemia cell samples 48 h after treatment and controls. The increase in T_{1obs} is consistent with similar measurements made previously on the same cell line at 3 T at the 36 h time point (4), as well as the late-stage apoptotic changes observed in vivo in rat glioma at 2 T (5) and 4.7 T (26), although those changes were largely attributed to a change in water density that cannot be mimicked fully with this in vitro model.

Although the fraction of macromolecular protons, M_{0B}, appears to decrease, this number is, by definition, relative to the fraction of free water protons, M_{0A}, which has been normalized to one in all cases here. Therefore, the observed decrease may be due to an increase in the free water content rather than a loss of macromolecular exchange sites. For example, previous studies using this in vitro model demonstrated an increase in the extracellular water fraction from 14 to 32% (4). For a constant intracellular water fraction (which is not entirely accurate; there is a small decrease in cell size during apoptosis), this would alter the M_{0B} value from 4.4% for controls to 3.5% simply because of increase in extracellular water. The value of M_{0B} in this study at the 36 h time point was 3.8 ± 1.2 %, indicating that the observed change may be due largely to increased free water content rather than a decrease in the number of macromolecular exchange sites.

Although the fitted curves all qualitatively appear like those of Fig. 1, with the 36 h apoptotic time point falling below controls and the 48 h time point falling below both of these, the change in MTR was not statistically significant at the 2.32 kHz offset frequency. The sensitivity was improved by incorporating information across frequencies and calculating $R \times M_{0B}/R_{1A}$. The $R \times M_{0B}$ factor describes the decrease in water signal because of exchange with saturated protons from the macromolecular pool, whereas R_{1A} describes the competing recovery effect because of T_1 relaxation of the free water pool. Although M_{0B} contributes a small decrease to the ratio, the decrease in R_{1A} is the dominant contributor, producing an increase in $R \times M_{0B}/R_{1A}$ and increasing the MT effect observed in the curve.

Thus, although there is a change in the MT spectrum, the model parameters that change significantly are largely related to the free water pool: a decrease in R_{1A}

and an increase in T_{2A}. Even the change in M_{0B} may be due to an increase in free water, decreasing the relative number of macromolecular protons.

There are several considerations in translating this work in vivo. First, the apoptotic fractions observed here, 0.35 $\pm$ 0.24 at early stages of apoptosis and 0.68 $\pm$ 0.14 at late stages are larger than those typically seen in vivo. Studies in responding patients have shown a 2–6-fold increase over the baseline apoptotic values of a few percent (1), which will decrease the sensitivity of this method.

The extracellular volume fraction may also differ. In vivo, cells shrink within the space they originally occupied and there may be an influx of water. In this in vitro model, cells are centrifuged after undergoing the morphological changes of apoptosis, minimizing the effect of water influx. Furthermore, there is no clearance by macrophages in vitro. Changes in extracellular water fraction are due only to changes in cell size and in cell packing from cell shape changes. The change in extracellular water fraction in vivo may, therefore, be larger, increasing the sensitivity of the MT parameters related to the free water pool.

However, methods such as diffusion, T_1 and T_2, which are sensitive to the amount of extracellular space and water content (5,6), may be more straightforward methods of detecting apoptosis, with lower RF energy deposition and potentially shorter measurement times. This is demonstrated by the T_{1obs} values in this study (Fig. 2a), which show a statistically significant increase at the same point in the apoptotic process as the MT changes become observable. MT at higher fields, where the T_1 relaxation time tends to be longer, might increase sensitivity to the macromolecular pool and thus to intracellular changes that provide complementary information to water content changes during apoptosis.

CONCLUSIONS

This study showed an increased MT effect in cell samples undergoing apoptosis. The effect is not significant at the measured signal-to-noise ratio levels until late apoptotic stages, 48 h after induction of cell death in this study, the point at which nuclear fragmentation and membrane blebbing become evident. Quantitative fittings of the MT spectrum indicate a significant increase in the T_2 of free water and a decrease in the relative fraction of macromolecular protons, which may be due in part to water influx. This indicates that MT may be a marker of apoptosis and allow early detection of the efficacy of cancer therapies, but the MT changes largely reflect changes in the free water pool.

ACKNOWLEDGMENTS

We would like to thank Anoja Giles for advice on cell culture. The author C.B. was supported by National Sciences and Engineering Research Council.

REFERENCES

1. Symmans WF, Volm MD, Shapiro RL, Perkins AB, Kim AY, Demaria S, Yee HT, McMullen H, Oratz R, Klein P, Formenti SC, Muggia F. Paclitaxel-induced apoptosis and mitotic arrest assessed by serial fine-needle aspiration: implications for early prediction of breast cancer response to neoadjuvant treatment. Clin Cancer Res 2000;6: 4610–4617.
2. Ellis PA, Smith IE, McCarthy K, Detre S, Salter J, Dowsett M. Preoperative chemotherapy induces apoptosis in early breast cancer. Lancet 1997;349:849.
3. Scott CE, Adebodun F. 13C-NMR investigation of protein synthesis during apoptosis in human leukemic cell lines J Cell Physiol 1999; 181:147–152.
4. Bailey C, Giles A, Czarnota GJ, Stanisz GJ. Detection of apoptotic cell death in vitro in the presence of gd-DTPA-BMA. Magn Reson Med 2009;62:46–55.
5. Chenevert TL, McKeever PE, Ross BD. Monitoring early response of experimental brain tumors to therapy using diffusion magnetic resonance imaging. Clin Cancer Res 1997;3:1457–1466.
6. Valonen PK, Lehtimaki KK, Vaisanen TH, Kettunen MI, Grohn OH, Yla-Herttuala S, Kauppinen RA. Water diffusion in a rat glioma during ganciclovir-thymidine kinase gene therapy-induced programmed cell death in vivo: correlation with cell density. J Magn Reson Imaging 2004;19:389–396.
7. Li J, Eastman A. Apoptosis in an interleukin-2-dependent cytotoxic T lymphocyte cell line is associated with intracellular acidification. Role of the na(+)/H(+)-antiport. J Biol Chem 1995;270:3203–3211.
8. van Tilborg GAF, Mulder WJM, Deckers N, Storm G, Reutelingsperger CPM, Strijkers GJ, Nicolay K. Annexin A5-functionalized bimodal lipid-based contrast agents for the detection of apoptosis. Bioconjug Chem 2006;17:741–749.
9. Petrovsky A, Schellenberger E, Josephson L, Weissleder R, Bogdanov A Jr. Near-infrared fluorescent imaging of tumor apoptosis Cancer Res 2003;63:1936–1942.
10. Kartachova MS, Valdes Olmos RA, Haas RL, Hoebers FJ, van den Brekel MW, van Zandwijk N, Herk M, Verheij M. Mapping of treatment-induced apoptosis in normal structures: 99mTc-hynic-rh-annexin V SPECT and CT image fusion. Eur J Nucl Med Mol Imaging 2006;33:893–899.
11. Blankenberg FG, Katsikis PD, Storrs RW, Beaulieu C, Spielman D, Chen JY, Naumovski L, Tait JF. Quantitative analysis of apoptotic cell death using proton nuclear magnetic resonance spectroscopy. Blood 1997;89:3778–3786.
12. Brisdelli F, Iorio E, Knijn A, Ferretti A, Marcheggiani D, Lenti L, Strom R, Podo F, Bozzi A. Two-step formation of 1H NMR visible mobile lipids during apoptosis of paclitaxel-treated K562 cells. Biochem Pharmacol 2003;65:1271–1280.
13. Milkevitch M, Shim H, Pilatus U, Pickup S, Wehrle JP, Samid D, Poptani H, Glickson JD, Delikatny EJ. Increases in NMR-visible lipid and glycerophosphocholine during phenylbutyrate-induced apoptosis in human prostate cancer cells. Biochim Biophys Acta 2005;1734: 1–12.
14. Stanisz GJ, Kecojevic A, Bronskill MJ, Henkelman RM. Characterizing white matter with magnetization transfer and T2. Magn Reson Med 1999;42:1128–1136.
15. Makela HI, Kettunen MI, Grohn OH, Kauppinen RA. Quantitative T(1rho) and magnetization transfer magnetic resonance imaging of acute cerebral ischemia in the rat. J Cereb Blood Flow Metab 2002; 22:547–558.
16. Lemaire L, Franconi F, Saint-Andre JP, Roullin VG, Jallet P, Le Jeune JJ. High-field quantitative transverse relaxation time, magnetization transfer and apparent water diffusion in experimental rat brain tumour. NMR Biomed 2000;13:116–123.
17. Liepinsh E, Otting G. Proton exchange rates from amino acid side chains—implications for image contrast. Magn Reson Med 1996;35: 30–42.
18. Gupta RK, Ferretti JA, Becker ED, Weiss GH. A modified fast inversion-recovery technique for spin-lattice relaxation measurements. J Magn Reson 1980;38:447–452.
19. Sled JG, Pike GB. Quantitative interpretation of magnetization transfer in spoiled gradient echo MRI sequences. J Magn Reson 2000;145: 24–36.
20. Sled JG, Pike GB. Quantitative imaging of magnetization transfer exchange and relaxation properties in vivo using MRI, Magn Reson Med 2001;46:923–931.
21. Morrison C, Henkelman RM. A model for magnetization transfer in tissues. Magn Reson Med 1995;33:475–482.
22. Henkelman RM, Huang X, Xiang QS, Stanisz GJ, Swanson SD, Bronskill MJ. Quantitative interpretation of magnetization transfer. Magn Reson Med 1993;29:759–766.

23. Bevington,PR, Robinson,DK. Data reduction and error analysis for the physical sciences. Boston: McGraw-Hill; 2003. p320.
24. Duvvuri U, Poptani H, Feldman M, Nadal-Desbarats L, Gee MS, Lee WM, Reddy R, Leigh JS, Glickson JD. Quantitative T1rho magnetic resonance imaging of RIF-1 tumors in vivo: detection of early response to cyclophosphamide therapy. Cancer Res 2001;61:7747–7753.
25. Grohn OH, Valonen PK, Lehtimaki KK, Vaisanen TH, Kettunen MI, Yla-Herttuala S, Kauppinen RA, Garwood M. Novel magnetic resonance imaging contrasts for monitoring response to gene therapy in rat glioma. Cancer Res 2003;63:7571–7574.
26. Hakumaki JM, Grohn OH, Tyynela K, Valonen P, Yla-Herttuala S, Kauppinen RA. Early gene therapy-induced apoptotic response in BT4C gliomas by magnetic resonance relaxation contrast T1 in the rotating frame. Cancer Gene Ther 2002;9:338–345.
27. Sierra A, Michaeli S, Niskanen JP, Valonen PK, Grohn HI, Yla-Herttuala S, Garwood M, Grohn OH. Water spin dynamics during apoptotic cell death in glioma gene therapy probed by T(1rho) and T(2rho). Magn Reson Med 2008;59:1311–1319.
28. Portnoy S, Stanisz GJ. Modeling pulsed magnetization transfer. Magn Reson Med 2007;58:144–155.